DESIGN AND EXPERIMENT OF A SMALL SELF-PROPELLED LIQUID-FERTILIZER INJECTOR

/

小型自走式液肥注射机设计与试验

Ting GUO[1)], Xi XIAO[1)], Ming LIU[2)], Chengsong LI[2)], Linji LI[1)], Lin ZHU[1)], Wanneng LI[*2)]
[1)] Hunan Provincial Tobacco Company, Chenzhou City Company, Hunan / China
[2)] College of Engineering and Technology, Southwest University, Chongqing / China
Tel: +86 13102054853; E-mail: 19822514833@163.com
Corresponding author: Wanneng Li
DOI: https://doi.org/10.35633/inmateh-79-53

Keywords: *Liquid fertilizer, Precision deep fertilization, Crank-slider injection mechanism, Computational fluid dynamics*

ABSTRACT

To address the limited maneuverability and terrain adaptability of conventional liquid-fertilizer injection equipment in hilly and small-plot farmland, a compact self-propelled injector integrating a narrow-track four-wheel-drive chassis, an angle-adjustable injection unit, and a crank-slider penetration mechanism was developed. Unlike large tractor-mounted or fixed-orientation systems, the proposed machine integrates inter-row movement, posture adjustment, needle penetration, and timed point injection on a lightweight platform. The discharge characteristics of the injection needle were investigated using computational fluid dynamics, and a three-factor, three-level Box–Behnken design was employed to optimize injection duration, inlet pressure, and outlet-hole number, with fertilizer volume per injection as the response. Response surface optimization identified an injection duration of 1 s, an inlet pressure of 0.45 MPa, and six outlet holes as the preferred parameter combination. Field validation yielded a measured fertilizer volume of 675.4 mL per injection, compared with the predicted value of 700 mL, corresponding to a relative difference of 3.51%. The results demonstrate the feasibility of controllable deep point placement under the tested conditions and provide a lightweight equipment solution for liquid-fertilizer application in hilly and small-plot farmland.

摘要

针对传统液肥注射施肥装备在丘陵山区及小地块农田中机动性和地形适应性不足的问题，研制了一种集窄距四轮驱动底盘、角度可调式注射单元和曲柄滑块入土机构于一体的小型自走式液肥注射机。与大型拖拉机悬挂式或固定姿态作业系统相比，该机可在轻量化平台上实现行间行走、姿态调节、施肥针入土及定时定点注肥。采用计算流体动力学方法分析施肥针排液特性，并以单次注肥体积为响应值，开展三因素三水平 Box–Behnken 响应面试验，对注肥时间、入口压力和出液孔数进行优化。响应面优化得到较优参数组合为注肥时间 1 s、入口压力 0.45 MPa 和出液孔数 6 个。田间验证中，单次注肥体积实测值为 675.4 mL，模型预测值为 700 mL，相对误差为 3.51%。结果表明，所研制机具在试验条件下能够实现可控的液肥定点深施，可为丘陵山区及小地块农田液肥机械化施用提供轻量化装备方案。

INTRODUCTION

In agricultural production, fertilizers are mainly applied in solid and liquid forms. Solid fertilizers are widely used, but their slow nutrient release and prolonged crop uptake often result in low utilization efficiency and considerable nutrient loss. In contrast, liquid fertilizers have the advantages of rapid nutrient release, high absorption efficiency and low application cost, making them suitable for crop topdressing *(Zhou et al., 2023)*. However, surface or shallow application of liquid fertilizer is prone to volatilization and nutrient loss, which reduces fertilization efficiency and limits crop yield improvement *(Hu et al., 2016)*. Previous studies have shown that deep point placement of liquid fertilizer can reduce nutrient loss, improve fertilizer use efficiency, mitigate environmental pollution and promote crop yield *(Li et al., 2018)*.

Liquid fertilizer is commonly applied through drip irrigation, foliar spraying and subsurface placement. Among subsurface application methods, band placement and point placement are the two main modes. Deep-placement technology for liquid fertilizer has been investigated relatively early in other countries and various dedicated applicators have been developed to improve application accuracy and fertilizer utilization.

For example, a soil-punching liquid-fertilizer applicator was developed to keep the injection needle vertical during soil penetration and withdrawal, thereby enabling fixed-point injection *(da Silva et al., 2017)*. An injection dosing system for site-specific liquid-fertilizer management was also designed by synchronizing soil punching and liquid-fertilizer injection to improve placement accuracy *(da Silva and Magalhães, 2019)*. In addition, precision injection of dairy sludge in no-till silage corn was reported to improve nutrient uptake under injection placement *(Hunt and Bittman, 2021)*. More recently, a liquid-manure point-injection system was designed and tested under field conditions, showing that subsurface injection could reduce nitrogen losses *(Hesar et al., 2025).*

In China, considerable efforts have also been made to develop liquid-fertilizer deep-placement equipment. The 3SFBQ-500 pneumatic blasting soil-loosening and fertilization machine can achieve fixed-point fertilization at depths of 200–500 mm in orchard hard soil through the coordinated operation of a drilling rod and a fertilizer injection unit *(Xi et al., 2017; Xi, 2018)*. Several liquid-fertilizer point-application devices have been developed, including the 1YJ-140 deep-placement applicator, in which the punching component was driven by a crank-rocker mechanism and the transmission system was improved to enhance operating efficiency *(Wang et al., 2016, 2017, 2018)*. Nevertheless, severe vibration still occurred under high-frequency operating conditions *(Feng et al., 2017; Liu et al., 2016)*. A liquid-fertilizer applicator for maize topdressing was also developed to improve fertilization efficiency and field adaptability by using multiple injection needles and a ground-clearance adjustment mechanism *(Xing, 2019)*.

Although substantial progress has been made in quantitative deep placement of liquid fertilizer, existing equipment still has several limitations, including large machine size, inconvenient transport, and poor adaptability to complex terrain. These limitations restrict its application in hilly areas and small plots, where low mass, flexible mobility, posture adjustment, and stable needle penetration are required *(Sun, 2024)*. Moreover, previous studies have focused mainly on tractor-mounted or fixed-orientation systems, whereas integrated solutions that combine terrain adaptation, injection-posture adjustment, and intermittent point application on a lightweight self-propelled platform remain limited.

The main methodological contribution of this study is the integration of CFD-based internal-flow analysis with Box–Behnken response surface optimization to quantify the individual and interactive effects of injection duration, inlet pressure, and outlet-hole number on fertilizer volume per injection. The principal engineering contribution is the integration of a four-wheel-drive narrow-track chassis, a rotary–tilting posture-adjustment platform, and a crank-slider injection mechanism into a compact 45 kg machine. Structural design, mechanical analysis, CFD simulation, parameter optimization, and field validation were combined to evaluate the feasibility of controllable deep point placement in hilly and fragmented farmland.

MATERIALS AND METHODS

Structural design and working principle

The overall structure of the small self-propelled liquid-fertilizer injector is shown in Fig. 1. The machine mainly consists of a narrow-track chassis, an adjustable tilting platform, a rotary adjustment platform, a crank-slider injection mechanism, a guide support mechanism, and a liquid-fertilizer delivery system.

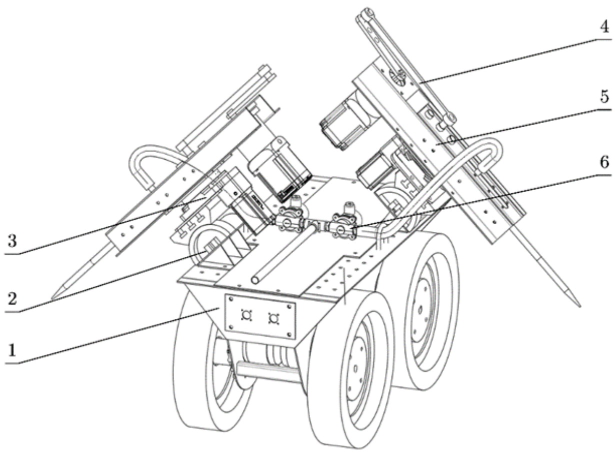

Fig. 1 - Overall structure of the small self-propelled liquid-fertilizer injector

1 - Narrow-track chassis; 2 - Adjustable tilting platform; 3 - Rotary adjustment platform

4 - Crank-slider injection mechanism; 5 - Guide support mechanism; 6 – Liquid-fertilizer delivery system

During operation, the injector is remotely guided into the inter-row space, and the liquid-fertilizer pipeline is connected to the pump. After automatic mode is activated, the machine moves to the preset fertilization position, where the rotary adjustment platform turns through 90 degrees to orient the injection unit perpendicular to the ridge slope (Fig. 2a). The stepper motor then drives the crank-slider mechanism, causing the injection needle to penetrate the soil to the preset depth (Fig. 2b). Once the needle reaches the target position, the solenoid valve opens, and pressurized liquid fertilizer is delivered through the needle into the soil. The needle then retracts, and the machine advances to the next position (Fig. 2c). Repetition of this sequence enables fixed-point deep placement of liquid fertilizer.

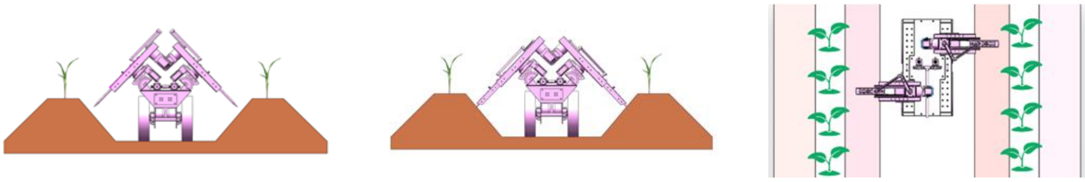

a) b) c)

Fig. 2 - Operating process of the small self-propelled liquid-fertilizer injector

Table 1

Main technical parameters of the machine

Item	Technical parameters
Overall dimensions / mm	810 × 430 × 500
Machine mass / kg	45
Narrow-track chassis motor / N·m	0.98
Holding torque of crank drive motor / N·m	80
Driving torque of rotary platform motor / N·m	2.2
Number of injection needles	2
Injection depth / mm	100–200

Design of key components and mechanical analysis

Narrow-track chassis

To improve passability and driving stability on wet, muddy and uneven terrain, the narrow-track chassis was equipped with a four-wheel electric drive system. Compared with a conventional two-wheel-drive configuration, four-wheel drive provides greater traction and improved terrain adaptability, thereby enhancing machine stability under complex field conditions *(Jiang et al., 2025)*. As shown in Fig. 3, the chassis mainly consists of an anti-collision beam, motor reducers, drive motors, a socket plate, triangular inclined plates, waterproof plates, a frame, wheels and flanges.

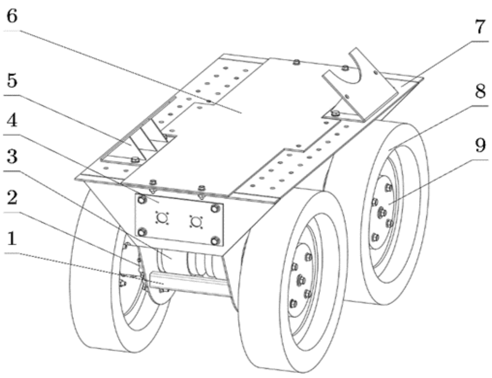

Fig. 3 – Structure of the narrow-track chassis

1 – Anti-collision beam; 2 – Motor reducer; 3 – Drive motor; 4 - Socket plate; 5 – Triangular inclined plate; 6 – Waterproof plate; 7 – Frame; 8 – Wheel; 9 – Flanges

According to China's third national land survey, farmland slopes generally range from 0 to 15 degrees *(People’s Daily, 2021)*. Based on the operating conditions of tobacco fields in Guiyang County, Hunan Province, the design slope was set to 10°. The chassis was therefore required to climb a 10-degree slope steadily at 2 km·h^{-1}. A brushed DC motor was selected as the chassis power source, and its principal parameters are listed in Table 2.

Table 2

Main technical parameters of the motor

Item	Parameter
Rated power / kW	0.25
Rated torque / N·m	0.64–0.98
Rated speed / r/min	2400–3700
Maximum speed / r/min	3700
Rated current / A	13.4
Motor efficiency / %	70

Angle-adjustable injection unit

The angle-adjustable injection unit is the core component of the small self-propelled liquid-fertilizer injector, and its structure and operating parameters directly affect injection performance. As shown in Fig. 4, the unit mainly consists of an injection needle, sliding rail, crank-slider mechanism, drive motor, rotary adjustment platform and adjustable tilting platform. Needles with different lengths and diameters can be selected according to crop requirements, while the combined use of the rotary adjustment platform and adjustable tilting platform enables deep placement under different terrain and angular conditions.

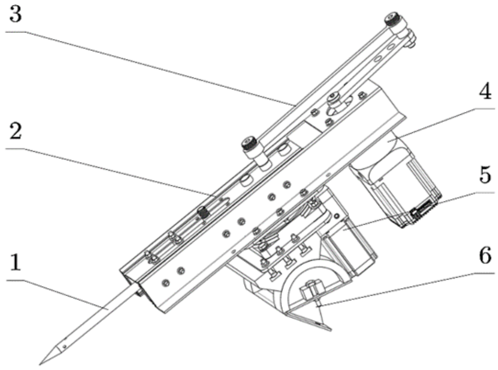

Fig. 4 - Structure of the angle-adjustable injection unit

1 - Injection needle; 2 - Sliding rail; 3 - Crank-slider injection mechanism; 4 - Drive motor; 5 - Rotary adjustment platform; 6 - Adjustable tilting platform

The injection needle directly affects fertilizer discharge through its internal flow channel and outlet geometry, particularly the number and diameter of the outlet holes. The required discharge performance was therefore evaluated through theoretical analysis and CFD simulation to provide a basis for needle design and parameter optimization. For each operating condition, the mean discharge rate of one injection needle was calculated from the injection duration and fertilizer volume as follows:

$$Q_{needle} = \frac{V}{t} \tag{1}$$

where:

Q_{needle} is the mean discharge flow rate of one injection needle (mL/s), V is *the fertilizer volume* delivered during one injection cycle (mL), and t is the injection duration (s).

Under steady-flow conditions, the discharge from each outlet hole is governed mainly by the pressure difference and effective flow area. Therefore, a theoretical discharge relation was established based on the Bernoulli equation as follows:

$$Q = C_d \bullet A \bullet \sqrt{\frac{2\Delta P}{\rho}} \tag{2}$$

where:

Q is the instantaneous flow rate through one outlet hole (m^3/s), C_{d} is the discharge coefficient, A is the outlet-hole area (m^2), ΔP is pressure difference between the needle inlet and outlets (Pa), and ρ is the density of the liquid fertilizer, taken as 1085 kg/m^3.

To ensure stable soil penetration of the injection needle under field conditions, the soil properties and loading characteristics were analyzed. Soil samples were collected from tobacco fields in Guiyang County, Chenzhou City, Hunan Province, China. Field measurements showed that the soil firmness ranged from 125 to 145 PSI, corresponding to approximately 0.86–1.00 MPa, indicating a relatively compact tillage layer.

During needle penetration, the soil resistance is mainly composed of cohesion, compressive resistance, frictional resistance and adhesion. These components jointly determine the total penetration resistance that must be overcome by the injection needle. Based on the force and failure characteristics of soil during penetration, the resistance model of the injection needle was established as follows *(You et al., 2017)*:

$$P = N + T + C_a + C \tag{3}$$

where: N is the compressive component of soil resistance, T is the frictional component, C_a is the adhesive component and C is the cohesive component of soil resistance.

In Fig. 5, P is the insertion force, which is equal in magnitude to the penetration resistance of the injection needle. N_1, T_1 and Ca_1 represent the normal force, frictional force and tangential adhesion acting on the needle tip, respectively, while N_2, T_2 and Ca_2 are the corresponding forces acting on the needle wall. C is the soil cohesive force.

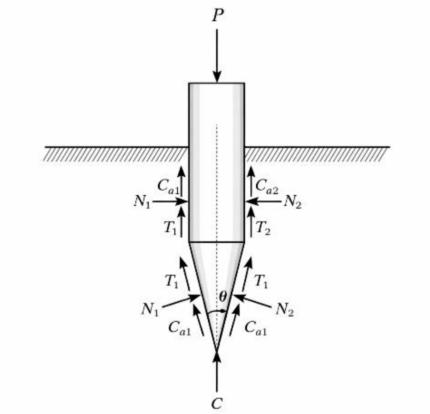

Fig. 5 - Force analysis of the injection needle during soil penetration

The penetration resistance analysis showed that the injection needle must overcome considerable soil resistance during insertion. Therefore, the injection mechanism should provide sufficient driving force while ensuring stable reciprocating motion at the required depth. In this study, an in-line crank-slider mechanism was adopted for the injection unit, as shown in Fig. 6. The mechanism has a simple structure, reliable transmission and good motion stability, and can convert the continuous rotary motion of the motor into the reciprocating linear motion of the injection needle, which is suitable for intermittent liquid-fertilizer deep placement.

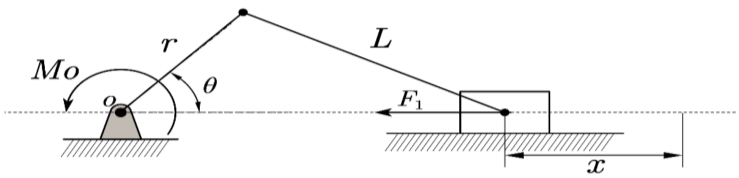

Fig. 6 - Crank-slider injection mechanism

The crank-slider injection mechanism mainly consists of a motor, reducer, crank, connecting rod, slider, and guide rail. According to the agronomic requirements and field operating conditions, the penetration depth of the injection needle was designed as 100–200 mm. To avoid interference between the needle and surface crops or mulch before soil entry, an idle-travel segment was included in the motion path. Therefore, the total slider stroke was designed to be no less than 300 mm, including 100 mm of idle travel and 100–200 mm of effective penetration depth. For the crank-slider mechanism, the slider stroke is determined by the crank radius and can be expressed as follows:

$$S = 2r \tag{4}$$

where: S is the slider stroke (mm) and r is the crank radius (mm).

According to the stroke requirement, the crank radius r was set to 160 mm, corresponding to a theoretical slider stroke of 320 mm. The connecting-rod length L was selected as 315 mm to achieve a compact layout and stable reciprocating motion.

Taking the crank center *O* as the coordinate origin, the horizontal and vertical directions were defined as the x- and y-axes, respectively. During needle penetration, the soil reaction force acting on the slider is transmitted to the crank through the connecting rod, thereby determining the torque requirement of the drive motor. The maximum penetration resistance calculated from the soil resistance model was taken as the design load. Based on the geometric constraints and static equilibrium of the crank-slider mechanism, the relationship among the required crank torque M_0, the penetration resistance F_1 and the connecting rod length L was established as follows:

$$M_0 = F_1 \bullet L \bullet \sin\theta \tag{5}$$

Control system

Due to the limited clearance of narrow ridge furrows and the uneven terrain in hilly areas, inter-row operation requires accurate positioning, stable motion, and safe control. Liquid-fertilizer deep placement also requires coordinated control of vehicle movement, injection-unit posture adjustment, needle penetration, and timed fertilizer injection. Therefore, an electronic control system based on a microcontroller unit (MCU) was developed for the small self-propelled liquid-fertilizer injector. The system forms a control chain comprising command input, signal processing, actuator driving, and status protection. As shown in Fig.7, it mainly consists of a remote controller, signal receiver, main control module, motor drivers, drive motors, solenoid valve, relays, and a 24 V battery.

Wireless remote control was adopted for human–machine interaction. Operator commands were transmitted to the MCU through the signal receiver, and the controller generated output signals according to the selected operating mode and preset logic. The travelling subsystem controlled the drive motors through motor drivers to achieve start–stop, steering, and speed regulation. The injection subsystem controlled the crank-slider drive motor and rotary stepper motor to complete posture adjustment and needle reciprocating motion. During injection, the relay actuated the solenoid valve according to the preset timing sequence, thereby enabling coordinated on–off control of liquid-fertilizer delivery.

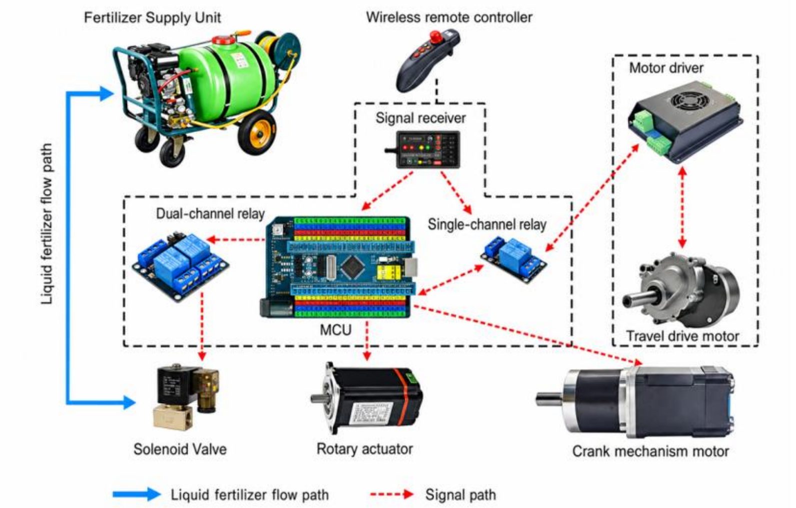

Fig. 7 - Hardware architecture of the control system

CFD simulation analysis of key components

To evaluate the discharge performance of the injection needle and quantify the effects of operating parameters on fertilizer volume per injection, a CFD model was established in ANSYS Fluent 2022 R1 *(Zawawi et al., 2018)*. The steady volumetric flow rate was obtained from the simulated outlet velocity field, and the fertilizer volume corresponding to a specified injection duration was calculated during post-processing using Eq. 7.

The liquid fertilizer was assumed to be an incompressible, single-phase Newtonian fluid uniformly supplied at the needle inlet. The internal flow was treated as steady, and gas–liquid interaction, evaporation, and particle transport were neglected. Under these assumptions, the flow was governed by the Reynolds-averaged continuity and momentum equations for an incompressible fluid.

$$\frac{\partial u}{\partial t}+(u\bullet\nabla)u=-\frac{1}{\rho}\nabla p+\nu\nabla^2 u \tag{6}$$

As shown in Fig.8, a three-dimensional model of the injection needle was created in SolidWorks 2021 and imported into ANSYS SpaceClaim and DesignModeler for geometry cleanup and internal flow-domain extraction. The computational domain was discretized using polyhedral cells in Fluent Meshing, with local refinement applied at the inlet and outlet-hole regions to resolve the relatively large velocity gradients near these boundaries.

A three-level mesh-independence test was conducted to assess the influence of mesh resolution on the numerical results. The four-outlet injection-needle model was evaluated at an inlet gauge pressure of 0.4 MPa, with all outlets maintained at 1 atm. Global mesh refinement was applied throughout the computational domain, while additional local refinement was imposed at the inlet and outlet regions to better resolve the flow gradients near these boundaries. The total volumetric flow rate through the four outlet holes was selected as the monitoring parameter. Except for the global and local mesh sizes and the resulting cell numbers, the geometry, fluid properties, boundary conditions, turbulence model, numerical schemes, and convergence criteria were kept unchanged. Therefore, differences in the calculated outlet flow rate were attributed solely to mesh refinement.

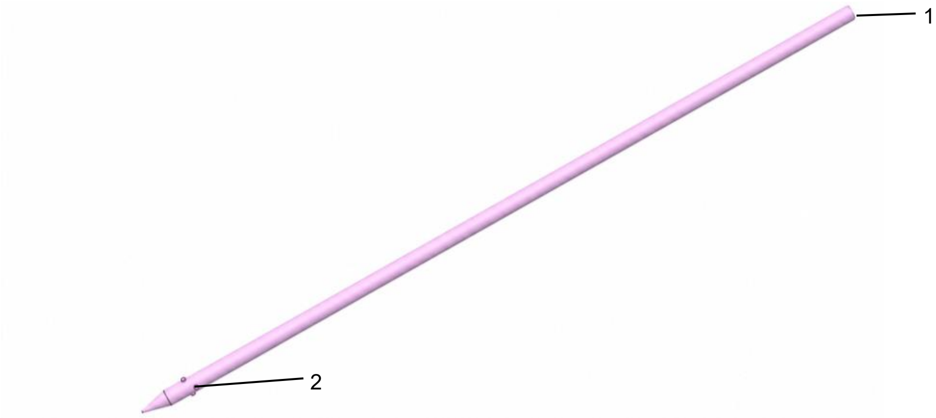

Fig. 8 - Three-dimensional model of the injection-needle flow domain

1 - inlet; 2 - outlet

Table 3

Mesh-independence assessment for the injection-needle internal-flow model

Mesh level	Global mesh size / mm	Local mesh size at the inlet and outlets / mm	Number of cells	Total outlet flow rate / (mL•s^{-1})
Coarse	0.60	0.07	550548	492.36
Medium	0.45	0.05	1565727	520.20
Fine	0.30	0.03	3495430	522.86

The total outlet flow rate increased from 492.36 mL·s-1 for the coarse mesh to 520.20 and 522.86 mL·s^{-1} for the medium and fine meshes, respectively. The relative difference between successive mesh levels decreased from 5.35% for the coarse-to-medium refinement to only 0.51% for the medium-to-fine refinement, demonstrating that further mesh refinement had a negligible influence on the predicted discharge performance. Accordingly, the medium mesh, with a global mesh size of 0.45 mm and a local mesh size of 0.05 mm at the inlet and outlet regions, was selected for subsequent simulations to achieve an appropriate balance between numerical accuracy and computational cost. The selected mesh comprised 1565727 polyhedral cells and 7322916 nodes.

The principal boundary conditions, fluid properties, and numerical settings used in the simulations are summarized in Table 4. In the Fluent post-processing stage, the fluid velocity at the outlet holes was used to calculate the volume as follows:

$$V = Q_v \bullet t = A \bullet v \bullet t \tag{7}$$

where: Q_v is the volumetric flow rate (m^3/s), A is the cross-sectional area through which fluid passes (m^2) and v is the fluid average velocity (m/s).

Table 4

Boundary conditions and numerical settings used in the CFD simulations

Item	Setting
Mesh	Polyhedral cells, global: 0.45 mm, inlet and outlet: 0.05 mm
Solver	Pressure-based, steady-state
Near-wall treatment	Standard wall functions
Turbulence model	Realizable *k-ε*
Pressure–velocity coupling	Coupled algorithm
Boundary conditions	Inlet: 0.2 - 0.6 MPa, outlet: 1 atm, no-slip walls
Fluid properties	ρ=1085 kg/m³, μ=1.05 × 10^{-3} Pa·s *(Zhang et al., 2018)*
Initialization	Standard initialization
Convergence criterion	Scaled residuals < 1 × 10^{-6}

A three-factor, three-level Box–Behnken design was generated using Design-Expert 13. Fertilizer volume per injection (Y_1) was taken as the evaluation index, while injection duration (X_1), injection pressure (X_2), and outlet-hole number (X_3) were selected as experimental factors. The factors and levels are listed in Table 5. In addition, velocity contours at the outlet holes under different working conditions were extracted to characterize the flow-field distribution in the outlet region. As an example, Fig. 9 shows the velocity contours obtained at an inlet pressure of 0.2 MPa with four outlet holes.

Table 5

Factors and levels for Box–Behnken design

Levels	Injection duration X_1 / (s)	Inlet pressure X_2 / (MPa)	Outlet-hole number X_3
-1	1	0.2	4
0	1.5	0.4	5
1	2	0.6	6

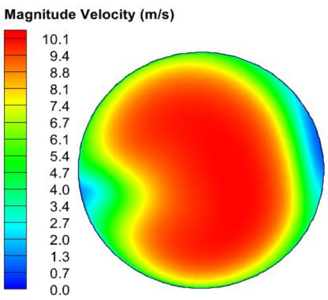

a) Velocity contour at outlet hole 1

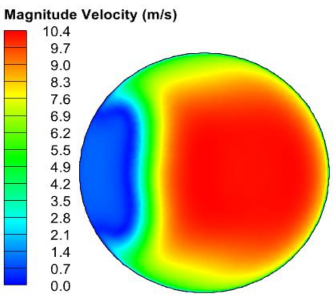

b) Velocity contour at outlet hole 2

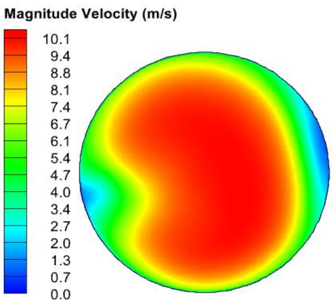

c) Velocity contour at outlet hole 3

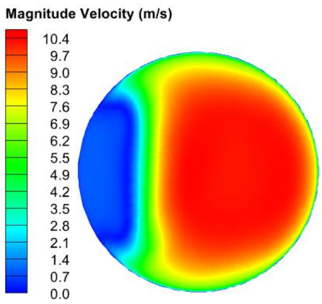

d) Velocity contour at outlet hole 4

Fig. 9 - Outlet velocity contours of the injection needle at 0.2 MPa with four outlet holes

RESULTS

Simulation results and analysis of variance

The Box–Behnken factor combinations and corresponding CFD responses are presented in Table 6.

Table 6

Box–Behnken design matrix and simulated responses

Run	X_1	X_2	X_3	Y_1
1	1.5	0.4	5	778.3
2	2.0	0.6	5	1640.3
3	1.5	0.6	4	1473.1
4	2.0	0.2	5	465.3
5	1.5	0.2	6	400.3
6	1.5	0.4	5	785.2
7	1.5	0.6	6	1220.3
8	1.0	0.4	4	520.2
9	1.5	0.4	5	853.3
10	1.5	0.4	5	815.9
11	1.0	0.6	5	1095.4
12	1.0	0.4	6	626.9
13	2.0	0.4	4	958.2
14	2.0	0.4	6	976.4
15	1.0	0.2	5	188.2
16	1.5	0.4	5	848.2
17	1.5	0.2	4	192.3

Design-Expert 13 was used to fit a quadratic polynomial model to Y_1 and perform analysis of variance. Injection duration (X_1), inlet pressure (X_2), and the interactions X_1X_2 and X_2X_3 had highly significant effects on fertilizer volume per injection, while the quadratic term X_2^2 was significant. The remaining terms were not significant, as shown in Table 7.

Table 7

ANOVA results for the fitted regression model of fertilizer volume per injection

Source	Sum of Squares	Df	Mean Square	F-value	*p*-value
Model	2.60E+06	9	2.89E+05	235.18	< 0.0001**
X_1	3.24E+05	1	3.24E+05	263.91	< 0.0001**
X_2	2.19E+06	1	2.19E+06	1782.58	< 0.0001**
X_3	802.4	1	802.4	0.654	0.4453
X_1X_2	17929.21	1	17929.21	14.61	0.0065**
X_1X_3	1958.06	1	1958.06	1.6	0.2469
X_2X_3	53088.77	1	53088.77	43.27	0.0003**
X_1^2	419.37	1	419.37	0.3418	0.5771
X_2^2	7112.46	1	7112.46	5.8	0.0469*
X_3^2	5388.84	1	5388.84	4.39	0.0743
Residual	8588.75	7	1226.96		
Lack of fit	3790.85	3	1263.62	1.05	0.4611
Pure error	4797.91	4	1199.48		
Cor total	2.61E+06	16			

Note: * indicates significance at $p < 0.05$; ** indicates significance at $p < 0.01$.

From the analysis of variance of the regression model, the second-order response regression equation for Y_1 was obtained as follows:

$$Y_1 = 816.18 + 201.19X_1 + 522.87X_2 + 10.01X_3 + 66.95X_1X_2 - 22.13X_1X_3 - 115.2X_2X_3 - 9.98X_1^2 + 41.1X_2^2 - 35.77X_3^2 \quad (8)$$

The model was highly significant, with a p-value below 0.01, an R^2 of 0.9967, an R^2_{adj} of 0.9925 and a CV of 4.30%, indicating an adequate fit for response-surface analysis and parameter optimization.

Response surface analysis

As shown in Table 7, the interaction terms X_1X_2 and X_2X_3 significantly affected fertilizer volume per injection, whereas X_1X_3 was not significant. Because X_2X_3 had the larger F-value, the response-surface analysis focused on the X_1X_2 and X_2X_3 interactions.

Figure 10a shows the interaction between injection duration and inlet pressure at a fixed outlet-hole number. Fertilizer volume per injection increased as both duration and pressure increased. The highest response occurred at the upper levels of both factors, whereas the lowest response occurred at the lower levels.

Figure 10b shows the interaction between inlet pressure and outlet-hole number at a fixed injection duration. Fertilizer volume per injection generally increased with inlet pressure, while the effect of outlet-hole number depended on the pressure level, consistent with the significant X_2X_3 interaction in Table 7.

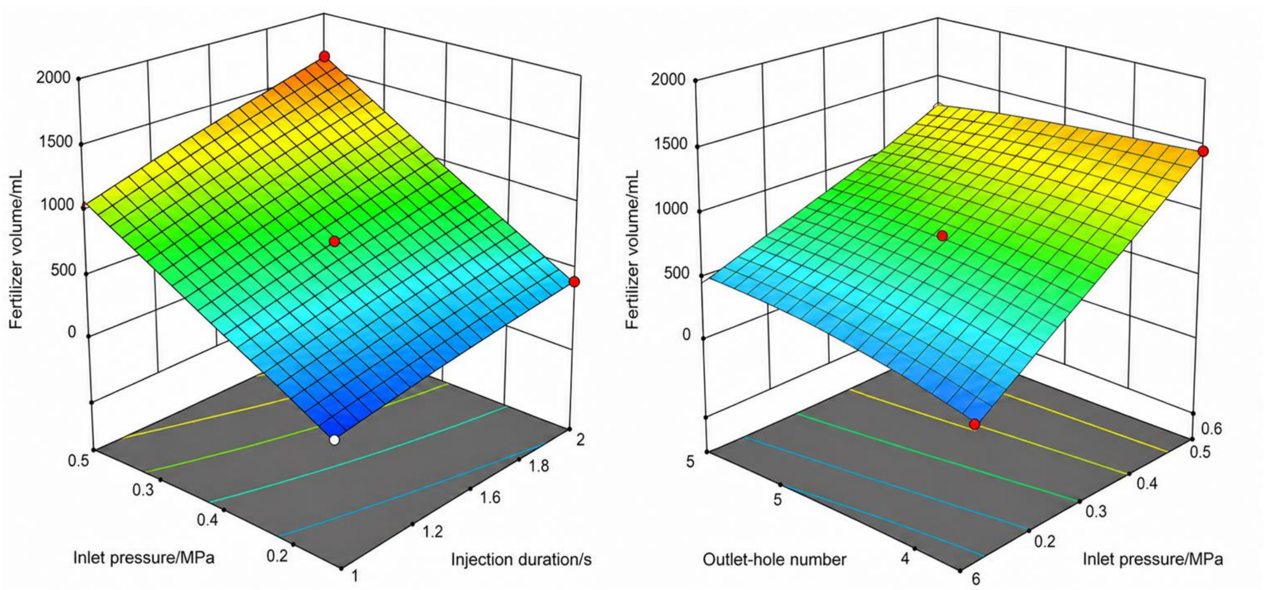

a) Response surface of the effects of X_1X_2 on Y_1 b) Response surface of the effects of X_2X_3 on Y_1

Fig. 10 - Interactive effects of the experimental factors on the evaluation indicator

For tobacco transplanting, the target fertilizer volume per injection was set at 700 mL, while injection duration was minimized to improve operating efficiency. Numerical optimization was performed in Design-Expert 13, with Y_1 set to a target value of 700 mL, X_1 minimized and X_2 and X_3 constrained within their respective design ranges. The resulting preferred parameter combination consisted of an injection duration of 1 s, an inlet pressure of 0.45 MPa, and six outlet holes.

Field test

To evaluate the field feasibility of the optimized parameter combination and compare the measured response with the model prediction, a field validation test was conducted in March 2025 at the Fangyuan Tobacco Research Base in Guiyang County, Chenzhou City, Hunan Province, China. The test object was flue-cured tobacco at the transplanting stage, as shown in Fig. 11. The test was carried out according to GB/T 43908-2024 Water and Fertilizer Integrated Equipment *(SAC/TC 201, 2024)*. During the test, the ambient temperature was 19.2–25.3°C, soil moisture was 24.3%–27.9%, soil pH was 6.05–6.23, and soil firmness was 0.827–0.965 MPa.

One tobacco row was randomly selected for field validation. The plant spacing, ridge-top width, ridge-bottom width, and ridge height were 450, 450, 750, and 300 mm, respectively. The injection direction was perpendicular to the ridge surface, and the injection depth was fixed at 150 mm.

The optimized settings consisted of an injection duration of 1 s, an inlet pressure of 0.45 MPa, and six outlet holes. Five independent injections were performed at spatially separated positions along the selected row. Fertilizer volume per injection was measured using a flowmeter, and the mean value was compared with the model prediction.

Fig. 11 - Field test

The measured fertilizer volume per injection was 675.4 mL, compared with the model prediction of 700 mL, corresponding to a relative error of 3.51%. The agreement between measured and predicted values verified the predictive accuracy of the response surface model under the tested field conditions.

DISCUSSION

Effects of operating parameters and model applicability

The dominant effect of inlet pressure was consistent with the Bernoulli-based discharge relation, according to which the outlet flow rate increases approximately with the square root of the pressure difference. At a given steady volumetric flow rate, fertilizer volume per injection increased approximately linearly with injection duration. Although outlet-hole number alone was not significant within the investigated range, its interaction with inlet pressure was highly significant. Because the diameter of each outlet hole was kept constant, increasing the number of holes increased the total discharge area. However, it also redistributed the internal pressure and altered the local hydraulic losses among the outlets. Therefore, the effect of outlet-hole number cannot be evaluated independently of inlet pressure. This result demonstrates the importance of multi-factor optimization rather than simply selecting the maximum level of each operating parameter.

The relative difference of 3.51% between the predicted and measured fertilizer volumes was probably associated with the response delay of the solenoid valve, transient pressure fluctuations during valve opening and closing, and pressure losses in the pipeline and connectors. These dynamic effects were simplified in the steady-state CFD model. Therefore, the present model provided an acceptable estimate of average discharge under the tested operating condition, but it did not fully characterize the transient start–stop injection process. Future work should incorporate transient CFD analysis and synchronized measurements of pressure and flow rate to improve the description of the dynamic fertilizer-delivery process.

Comparison with previously reported liquid-fertilizer applicators

Previous liquid-fertilizer applicators have mainly focused on soil-punching mechanisms, site-specific fertilizer dosing, injection-trajectory optimization, and subsurface placement under particular cropping systems. The soil-punching system developed by da Silva et al. *(2017)* maintained the injection needle in a nearly vertical orientation to achieve fixed-point application, whereas da Silva and Magalhães *(2019)* synchronized soil punching and fertilizer delivery for site-specific dosing. The mechanisms reported by Wang et al. *(2016, 2017, 2018)* improved punching trajectories and operating efficiency, although vibration remained a concern under high-frequency operation *(Feng et al., 2017; Liu et al., 2016)*. In comparison, the present injector was specifically configured for inter-row operation in hilly and fragmented farmland by integrating a 45 kg narrow-track self-propelled chassis, a rotary–tilting posture-adjustment platform, and a crank-slider injection mechanism.

Table 8

Comparison of the proposed injector with previously reported liquid-fertilizer applicators

Study	Application mode	Primary contribution	Application context
da Silva et al. *(2017)*	Soil punching	Fixed-point placement	Sugarcane fields
da Silva and Magalhães *(2019)*	Site-specific injection	Variable-rate dosing	Site-specific management
Wang et al. *(2016, 2017, 2018)*	Mechanical punching	Trajectory optimization	Mechanized field operation
Zhou et al. *(2023)*	Targeted deep application	Delivery control	Field crop production
Present study	Self-propelled point injection	Posture-adjustable placement	Hilly and small plots

Overall, the comparison shows that the principal distinction of the proposed injector lies in the integration of lightweight self-propelled mobility, posture adjustment, and controllable point injection for hilly and fragmented farmland. Unlike previous studies that mainly emphasized punching trajectories, dosing control, or application performance under specific cropping systems, the present design gives greater consideration to machine maneuverability and injection orientation. However, because the reported systems were evaluated using different crops, operating conditions, and performance indicators, Table 8 provides a qualitative comparison rather than a direct performance ranking.

Limitations and generalizability

Field validation was conducted at a single tobacco research site under a limited range of soil moisture, pH, and penetration resistance. The results therefore demonstrate feasibility under the reported conditions but should not be generalized directly to sandy, highly cohesive, stony, or waterlogged soils. Soil texture, moisture content, bulk density, and compaction may affect needle penetration, liquid distribution in soil, and machine traction. Multi-site experiments covering different soil types, slope gradients, and moisture conditions are required to establish broader applicability. Future studies should also evaluate long-term durability, energy consumption, leakage, operational reliability, and crop-response benefits.

CONCLUSIONS

(1) A lightweight self-propelled liquid-fertilizer injector integrating a four-wheel-drive narrow-track chassis, a rotary–tilting posture-adjustment platform, and a crank-slider injection mechanism was developed for hilly and small-plot farmland. The compact configuration enabled controllable needle penetration and timed point injection while supporting inter-row maneuverability and terrain adaptation.

(2) The combined CFD-based discharge analysis and Box–Behnken response surface optimization quantified the individual and interactive effects of injection duration, inlet pressure, and outlet-hole number on fertilizer volume per injection. Inlet pressure and injection duration were identified as the dominant factors. Field validation under the tested condition showed satisfactory agreement between the predicted and measured fertilizer volumes.

(3) The developed injector provides an engineering reference for lightweight precision deep-placement equipment in fragmented hilly farmland and may support the development of similar systems for tobacco and other row crops. Because validation was limited to one site and one soil condition, further studies should evaluate machine performance under different soil textures, moisture contents, and slope conditions.

ACKNOWLEDGEMENT

This research was funded by the Chenzhou Tobacco Company of Hunan Province under the project Development of a Lightweight Tobacco Ridging Machine for the Nanling Hilly Region (CZYC2022JS05).

REFERENCES

[1] da Silva M.J., Franco H.C.J., Magalhães P.S.G., (2017), Liquid fertilizer application to ratoon cane using a soil punching method, Soil and Tillage Research, vol.165, pp.279-285. DOI: https://doi.org/10.1016/j.still.2016.08.020

[2] da Silva M.J., Magalhães P.S.G., (2019), Modeling and design of an injection dosing system for site-specific management using liquid fertilizer, Precision Agriculture, vol.20, no.4, pp.649-662. DOI: https://doi.org/10.1007/s11119-018-9602-5
[3] Feng J.L., Wang J.W., Zhou W.Q., Tang H., Liu C.X., (2017), Design and optimization of operating parameters for a punching mechanism with deformed elliptical gears (变形椭圆齿轮式扎穴机构设计与工作参数试验优化), Transactions of the Chinese Society for Agricultural Machinery, vol.48, no.4, pp.90-96. DOI: https://doi.org/10.6041/j.issn.1000-1298.2017.04.011
[4] Hesar L.G., İnce A., Ekinci K., Gücüm H., (2025), Design and effectiveness of an injection system for the application of liquid manure (slurry) to soil, Journal of Agricultural Engineering, vol.57, no.1. DOI: https://doi.org/10.4081/jae.2025.1912
[5] Hu H., Zhang Y.F., Chen W.Z., Zhao H.B., (2016), Current status and future prospects of maize topdressing machinery in China (我国玉米追肥机械发展现状与前景展望), Journal of Maize Sciences, vol.24, no.3, pp.147-152. DOI: https://doi.org/10.13597/j.cnki.maize.science.20160323
[6] Hunt D.E., Bittman S., (2021), Precision injection of dairy sludge on crop yield and N and P uptake in juvenile and mature no-till silage corn, Agronomy, vol.11, no.2, article 370. DOI: https://doi.org/10.3390/agronomy11020370
[7] Jiang Y., Wang R., Ding R., Sun Z., Jiang Y., Liu W., (2025), Research review of agricultural machinery power chassis in hilly and mountainous areas, Agriculture, vol.15, no.11, article 1158. DOI: https://doi.org/10.3390/agriculture15111158
[8] Li X., Wu X.M., Zhang F.G., Fu D.L., He H.L., Nie Y., (2018), Design and experiment of a two-row deep fertilizer applicator for one ridge (一垄双行深施肥机的设计与试验), Journal of Agricultural Mechanization Research, vol.40, no.4, pp.110-115. DOI: https://doi.org/10.13427/j.cnki.njyi.2018.04.021
[9] Liu C.X., Wang J.W., Tang H., Zhou W.Q., Wang Q., Yang W.P., (2016), Dynamic analysis and experiment of a liquid fertilizer hole-punching mechanism based on a Bézier curve (基于贝塞尔曲线的液肥扎穴机构动力学分析与试验), Transactions of the Chinese Society for Agricultural Machinery, vol.47, no.5, pp.115-122. DOI: https://doi.org/10.6041/j.issn.1000-1298.2016.05.016
[10] Sun Q.H., (2024), Effects of integrated water and fertilizer management on tobacco yield and quality in the tobacco-growing area of southern Henan Province (豫南烟区水肥一体化施肥对烟草产量及品质的影响), MSc Thesis, Henan Agricultural University, Zhengzhou/China. DOI: https://doi.org/10.27117/d.cnki.ghenu.2024.000391
[11] Wang J.W., Zhang C.F., Zhou W.Q., Pan Z.W., Tang H., Duo T.Y., (2016), Optimization design of an irregular gear planetary punching mechanism based on MATLAB simulation (基于 MATLAB 仿真的非规则齿轮行星系扎穴机构的优化设计), Transactions of the Chinese Society of Agricultural Engineering, vol.32, no.3, pp.22-28. DOI: https://doi.org/10.11975/j.issn.1002-6819.2016.03.004
[12] Wang J.W., Zhou W.Q., Li X., Feng J.L., Jiang D.X., Wang J.F., (2018), Design and experiment of a variable-speed punching mechanism based on an oval-circular gear planetary train (卵形-全正圆齿轮行星系变速扎穴机构设计与试验), Transactions of the Chinese Society for Agricultural Machinery, vol.49, no.5, pp.136-142. DOI: https://doi.org/10.6041/j.issn.1000-1298.2018.05.015
[13] Wang J.W., Zhou W.Q., Wang X., Li X., Wang J.L., Li S.W., (2017), Study on an inclined punching mechanism based on trajectory fitting using a cubic Lagrange curve (基于三次拉格朗日曲线拟合轨迹的斜置式扎穴机构研究), Transactions of the Chinese Society for Agricultural Machinery, vol.48, no.5, pp.79-85. DOI: https://doi.org/10.6041/j.issn.1000-1298.2017.05.009
[14] Xi X.B., (2018), Research on pneumatic blasting soil loosening and fertilizer injection methods and equipment (气爆松土注肥方法及装备研究), PhD dissertation, Yangzhou University, Yangzhou/China.
[15] Xi X.B., Zhang R.H., Shan X., Jin Y.F., Zhang J.F., (2017), Optimization design and experiment of the 3SFBQ-500 orchard pneumatic blasting soil-loosening and fertilization machine (3SFBQ-500 型果园气爆松土注肥机的优化设计与试验), Transactions of the Chinese Society of Agricultural Engineering, vol.33, no.24, pp.35-43. DOI: https://doi.org/10.11975/j.issn.1002-6819.2017.24.005
[16] Xing X., (2019), Design of a liquid fertilizer applicator for maize (玉米液肥施肥机设计), MSc Thesis, Hebei Agricultural University, Baoding/China. DOI: https://doi.org/10.27109/d.cnki.ghbnu.2019.000047

[17] You Y., He C.B., Wang D.C., Wang G.H., (2017), Study on the interaction between extremely narrow tillage teeth and soil (土壤耕作部件极窄刀齿与土壤作用关系研究), Transactions of the Chinese Society for Agricultural Machinery, vol.48, no.6, pp.50-58. DOI: https://doi.org/10.6041/j.issn.1000-1298.2017.06.006
[18] Zawawi M.H., Saleha A., Salwa A., Hassan N.H., Zahari N.M., Ramli M.Z., Muda Z.C., (2018), A review: Fundamentals of computational fluid dynamics (CFD), AIP Conference Proceedings, vol.2030, no.1, article 020252. DOI: https://doi.org/10.1063/1.5066893
[19] Zhang X.H., Luo W.Y., Yang Y.J., Chen J.R., Yang Y.B., (2018), Effects of different nitrate nitrogen and ammonium nitrogen ratios on the yield and main chemical components of flue-cured tobacco (不同硝态氮和铵态氮配比对烤烟产量、主要化学成分的影响), Jiangxi Agriculture, no.24, pp.30-32. DOI: https://doi.org/10.19394/j.cnki.issn1674-4179.2018.24.028
[20] Zhou W., An T., Wang J., Fu Q., Wen N., Sun X., Wang Q., Liu Z., (2023), Design and experiment of a targeted variable fertilization control system for deep application of liquid fertilizer, Agronomy, vol.13, no.7, article 1687. DOI: https://doi.org/10.3390/agronomy13071687
[21] *** People’s Daily, (2021), Release of the main data results of the third national land survey (第三次全国国土调查主要数据成果发布), People’s Daily, p.17.
[22] *** SAC/TC 201, (2024), GB/T 43908-2024 Water and fertilizer integrated equipment, National Technical Committee for Agricultural Machinery Standardization, State Administration for Market Regulation and Standardization Administration of China, Beijing/China.